Sensors and Materials, Vol. 35, No. 12 (2023) 4215–4234
MYU Tokyo

S & M 3477

Electrochemical and Computational Studies of Citrate-modified β-cyclodextrin@Fe_3O_4 Nanocomposite as a Nonenzymatic Sensor for Cholesterol

Mochammad Arfin Fardiansyah Nasution, Metya Indah Firmanti, Hanzhola Gusman Riyanto, Afiten Rahmin Sanjaya, Endang Saepudin, and Tribidasari Anggraningrum Ivandini*

Department of Chemistry, Faculty of Mathematics and Natural Science, Universitas Indonesia, Depok 16424, Indonesia

(Received October 10, 2023; accepted December 6, 2023)

Keywords: cholesterol, non-enzymatic sensor, β-cyclodextrin (BCD), Fe_3O_4 nanoparticle, molecular docking simulation

A composite of citrate-modified β-cyclodextrin (CIT-BCD) and Fe_3O_4 was prepared by coprecipitation for a non-enzymatic cholesterol sensor application. Characterization using X-ray diffraction spectroscopy confirmed the spinel structure of Fe_3O_4, whereas infrared spectroscopy indicated that the composite of CIT-BCD@Fe_3O_4 was successfully synthesized. The cholesterol was detected on the basis of the competition of the inclusion complex formation between β-cyclodextrin (BCD) and cholesterol, and between BCD and methylene blue (MB), and the magnetic particles of Fe_3O_4 were used as the support medium of BCD. BCD was modified with citrate to improve its cholesterol loading capacity for a computational study through molecular docking simulation, which confirmed that cholesterol formed higher complex stabilities with both BCD and CIT-BCD than with MB, with the $\Delta G_{binding}$ values, of the complexes being −6.4 and −5.7 kcal/mol, respectively. A ratio of 3% (w/w) CIT-BCD@Fe_3O_4 nanocomposite and a contact time of 10 min were then found as optimum conditions. Furthermore, amperometric measurements performed using a screen-printed carbon electrode at an applied potential of −0.43 V (vs Ag/AgCl) with a measurement time of 90 s was conducted to detect the MB released from the system. Amperometry results showed good linearity ($R^2 > 0.99$) in the cholesterol concentration range of 0–100 μM with an estimated limit of detection of 3.93 μM. Good selectivity towards ascorbic acid, palmitic acid, tyrosine, and threonine was observed, whereas a significant change in current response was found in the presence of arginine. The developed method was successfully demonstrated to determine cholesterol levels in commercial corned beef samples. The method was also successfully validated by HPLC, indicating that the developed sensor is promising for real applications in cholesterol detection, especially in the matrix of meat samples.

*Corresponding author: e-mail: ivandini.tri@sci.ui.ac.id
https://doi.org/10.18494/SAM4698

ISSN 0914-4935
https://myukk.org/

1. Introduction

Cardiovascular disease (CVD) remains a major global health problem and the leading cause of death worldwide, with at least 16 million people dying owing to CVD each year.[1] In Indonesia, coronary heart disease and stroke rank first and second among the leading causes of death with the number of deaths reaching 5.9 and 5.2 million people in 2016, respectively.[2] To date, hypertension is still the most important factor contributing to the occurrence of CVD, and that hypertensive patients have a higher risk (by up to 50%) of suffering from heart attack, diabetes, and stroke.[3] Cholesterol [IUPAC name: (3β)-kolest-5-en-3-ol] is a sterol compound that serves as a precursor of various hormones and vitamin D.[4] Recent studies have shown that there is a correlation between the cholesterol concentration in the blood and coronary heart disease, that is, the higher the concentration of cholesterol in a person's blood, the higher the risk of having a heart attack.[5] Therefore, it is important, especially for those who suffer from hypertension, to maintain their cholesterol level to avoid the risk of CVD in the future.

To date, various instrumentation-based analysis methods have been commonly employed to detect the presence of cholesterol, such as chromatography methods,[6] enzymatic-based colorimetry,[7] and spectrophotometry.[8] However, these conventional methods have several shortcomings including low sensitivity, low time efficiency, and high maintenance costs.[9] To overcome these problems, cholesterol detection techniques were extensively studied and developed. One of the approaches is the development of a biosensor for cholesterol. The utilization of biosensors using enzymes is often combined with electrochemical techniques, owing to their high selectivity and sensitivity. In the case of cholesterol, various enzymes such as cholesterol oxidase, cholesterol esterase, and horseradish peroxidase have been widely used to detect the presence of cholesterol.[10] However, to maintain their effectiveness, the enzymes require specific treatments and storage. Thus, the required costs tend to be much higher. Therefore, the use of non-enzymatic biosensors as cholesterol detectors has also been widely studied and developed over the last few decades.

β-cyclodextrin (BCD) is a cyclic oligosaccharide compound formed from seven D-glucopyranose units connected by α-1,4 glycosidic bonds with a hydrophilic outer cavity and a hydrophobic inner cavity. Owing to its unique properties and high solubility in water, BCD has been extensively developed and plays a major role in the fields of catalyst development, supramolecular chemistry, food industry, drug delivery, and biosensor fabrication.[11–13] The application of BCD as a cholesterol biosensor has been studied using electrochemical techniques based on cyclic voltammetry (CV), amperometry, and enzyme-based electrodes[14–18] with methylene blue (MB) applied as a redox indicator to provide electrochemical signals.[18]

Furthermore, composites of BCD functionalized on magnetic nanoparticles, which combine the properties of the nanoparticles and the molecular recognition capability of BCD, have been widely used and have potential applications in the fields of medical diagnosis, magnetic separation, and controlled drug delivery.[18–21] The use of these composites as biosensors has been extensively studied as well.[19,22] On the other hand, it was reported that the modification of BCD with citrate improves the hydrophilic properties of BCD, leading to increases in its loading capacity and effectiveness when applied as a drug carrier of curcumin.[23] This result was

confirmed in a computational study that showed that citrate groups conjugated with BCD provide the highest binding affinity toward both cholesterol and MB among other functional groups.[24] Accordingly, in this work, the composite of citrate-modified BCD and the magnetic particles of Fe_3O_4 (CIT-BCD@Fe_3O_4) was synthesized for application as a cholesterol biosensor (Fig. 1). A computational study was also carried out through molecular docking simulation to reveal the binding affinity and molecular interactions that take place during the inclusion of BCD and CIT-BCD with cholesterol and MB. The results indicate that the modification of BCD@Fe_3O_4 with citrate groups increased the sensitivity of the developed cholesterol sensor. The sensor was successfully demonstrated to be capable of the determining the cholesterol level in a commercial corned beef sample, which was then validated by HPLC.

2. Research Methodology

2.1 Chemicals and materials

BCD (≥97%) and cholesterol (≥99%) were obtained from Sigma-Aldrich (Singapore), whereas MB and citric acid (CIT) (±99.5%) were purchased from Wako Pure Chemicals Ltd. (Osaka, Japan). Ammonium hydroxide (NH_4OH 25%), potassium hydrogen phosphate (K_2HPO_4), hydrochloric acid (HCl), absolute ethanol, ferric chloride hexahydrate ($FeCl_3 \cdot 6H_2O$), isopropanol, ferrous chloride tetrahydrate ($FeCl_2 \cdot 4H_2O$), potassium dihydrogen phosphate (KH_2PO_4), and sodium hydroxide (NaOH) were obtained from Merck (Darmstadt, Germany). All chemicals were used without further purification. For cholesterol detection, a locally and commercially available canned corned beef sample was used. Distilled water and double-distilled water were produced using Millipore Direct-Q® 8 UV and Millipore Direct-Q® 5 UV, respectively. For electrochemical measurements, a screen-printed carbon electrode (SPCE, DropSens DRP-110) from Metrohm Indonesia was used.

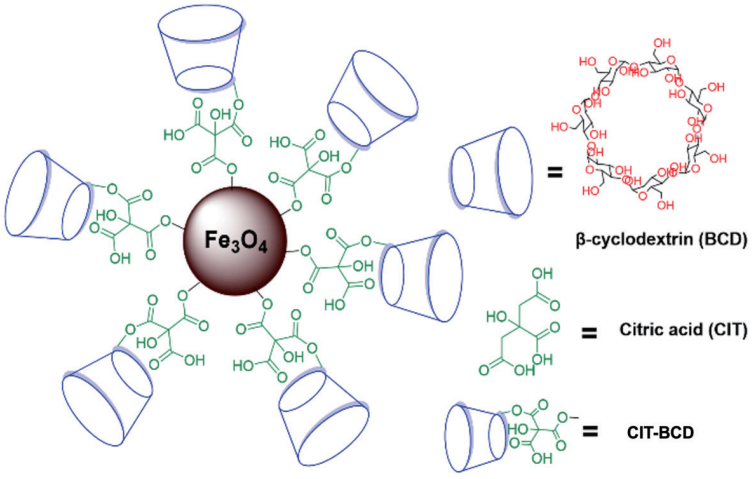

Fig. 1. (Color online) Scheme of intramolecular interactions between cholesterol and CIT-BCD@Fe_3O_4 nanocomposites.

2.2 Preparation and synthesis of CIT-BCD@Fe_3O_4 nanocomposite

The CIT-BCD complex was prepared according to a previous study.[18] Initially, 1.5 g of BCD and 0.5 g of CIT were dissolved in 10 mL of water, followed by vigorous stirring at 80 °C for 3 h. Then, the solution was washed with isopropanol until a white solid product formed, followed by centrifugation to separate the solid product from the solution by washing with isopropanol three times. Then, the obtained product was dried at 60 °C for 24 h and later characterized by Fourier transform infrared (FTIR) spectroscopy.

Fe_3O_4 nanoparticles were prepared according to previous studies.[18,25] Initially, 2 g of $FeCl_2.4H_2O$ and 5 g of $FeCl_3.6H_2O$ were added carefully to 100 mL of water that was previously heated at 80 °C. Then, a concentrated NH_4OH solution was slowly dropped into the solution until pH 11–12 was reached, followed by stirring for 30 min. After that, the solution was cooled for 30 min at room temperature, and the precipitate was washed with water and methanol before drying. The product was characterized by SEM-EDX and X-ray diffraction (XRD) spectroscopy.

The BCD@Fe_3O_4 nanocomposite was prepared on the basis of the previous research with modification.[23] Briefly, 1 g of Fe_3O_4 was added to 100 mL of water with heating at a temperature of 80 °C and stirring vigorously using a magnetic stirrer, wheras 0.5 g of CIT-BCD was slowly dissolved in 10 mL of water and then solutions were mixed. The mixture was then heated for 4 h at 80 °C.

The modified Fe_3O_4 nanoparticles were then collected using an external magnet, separated from the solvent, and dried using an oven for 24 h at 60 °C. As with Fe_3O_4, the nanocomposite was characterized by SEM-EDX and XRD spectroscopy. The CIT-BCD@Fe_3O_4 nanocomposite variants were synthesized by adding 10 mL each of 1, 2, and 3% (w/w) CIT-BCD and 1 g of Fe_3O_4 nanoparticles to 100 mL of water and then heated at 80 °C for 4 h with stirring.

2.3 Molecular docking simulation

Molecular docking simulation was performed to predict the molecular interactions between the respective complexes. First, the 3D structures of cholesterol and MB were obtained from the PubChem database (https://pubchem.ncbi.nlm.nih.gov/),[26] with PubChem CID: 5997 and 6099, respectively. Then, the BCD structure was obtained by elucidating the 3D structure of this compound from the SusD protein (PDB ID: 3CK8), obtained from the RCSB Protein Data Bank[27] using BIOVA Discovery Studio 2019 software. The structure of the BCD compound obtained was then saved in .pdb form. Finally, the CIT-BCD structure was obtained by substituting the H atom in the primary hydroxyl group (–OH) of the BCD structure with a citrate group. The CIT-BCD structure was then saved as a .pdb file format. All the structures obtained were then prepared by minimizing the structures obtained at the predocking stage.

The docking stage was carried out using PyRx 0.8.0 software by a method modified from previous methods.[28,29] The docking stage was further carried out using the AutoDock Vina module in the PyRx 0.8.0 software by utilizing MMFF94x as the main forcefield for the ligands. The grid box for the docking simulation was then determined at the lipophilic central cavity and the hydrophilic outer surface of both BCD and CIT-BCD. After that, the best confirmation from

the docking results with the lowest Gibbs binding energy ($\Delta G_{binding}$) and *RMSD* < 2 Å was selected as a representation of the docking results of BCD and CIT-BCD with both cholesterol and MB. All BCD and CIT-BCD inclusion complexes were stored in .pdb form. The results of docking in this study were further analyzed for the complex interaction of the inclusion using the BIOVA Discovery Studio 2019 software.

2.4 Electrochemical measurements of cholesterol

The electrochemical study of the sensors was carried out by investigating the optimized parameters for the cholesterol measurements, such as nanocomposite types [Fe_3O_4, CIT-BCD(1%)@Fe_3O_4, CIT-BCD(2%)@Fe_3O_4, CIT-BCD(3%)@Fe_3O_4], nanocomposite weights [1, 2, and 3% (w/w)], and contact times (5, 10, 15, and 20 min). Prior to the measurements, an MB-modified CIT-BCD@Fe_3O_4 (MB-CIT-BCD@Fe_3O_4) nanocomposite was prepared by adopting a previous method.[18] CIT-BCD@Fe_3O_4 of various weights was dispersed in 50 mM phosphate buffer solution (PBS; pH 7.4) and then sonicated for 10 min. Next, 2 mL of 0.5 mM MB solution was immobilized into 3 mL of the dispersed solution and kept for 3 h. The MB-CIT-BCD@Fe_3O_4 nanocomposite was obtained by removing the supernatant using an external magnet attached to the bottom of the flask. Then, the nanocomposite was washed with water.

The electrochemical study was performed using CV and amperometry techniques with SPCE. CV was carried out in the potential range from −0.6 to +0.6 V and at a scan rate of 40 $mV{\cdot}s^{-1}$, whereas amperometry was performed by applying a fixed potential at which the current was maximum. Initially, MB-CIT-BCD@Fe_3O_4 was dispersed in 400 μL of 50 mM PBS (pH 7.4) solvent and placed in an Eppendorf tube. Then, 100 μL of 100 μM MB was added and shaken by using a vortex. The tube was then placed in a rack with a magnet and 40 L of the solution was taken for amperometric measurement at a potential of −0.43 V using SPCE. Then, 40 μL of the solution containing cholesterol was added into the tube. The tube was shaken and allowed to stand for 10 min. A total of 40 μL of the solution that had been separated using an external magnet was taken, and the MB concentration in the remaining solution was remeasured by amperometry according to the previous parameters.

2.5 Cholesterol measurement in corned beef sample

The developed method was also examined for the detection of cholesterol content in a commercial corned beef sample and validated by using HPLC measurements. The sample was prepared by adding 1 mL of corned beef sample into a centrifuge tube followed by 20 mL of 0.5 M KOH in methanol solution. The tube was closed tightly and then immersed in a water bath at a temperature of 75 °C for 45 min. After cooling down to room temperature, 2 mL of water and 10 mL of n-hexane were added into the tube. The mixture was then sonicated for 20 min and centrifuged for 10 min. The top layer formed was separated and heated in the temperature range of 60–65 °C until around 5 mL of the sample remained. 0.5 mL of the remaining solution was taken and dissolved in a 5 mL volumetric flask with ethanol. Then, the solution was reheated in the temperature range of 60–65 °C until 5 mL of the sample remained. A volume of 40 μL of

this solution was used for amperometric measurements, whereas the percent recovery was obtained by measuring the sample with 40 μM cholesterol added.

As for the HPLC validation, the standard cholesterol curve was created by measuring 0, 20, 40, 60, 80, and 100 μM standard cholesterol solutions. The HPLC measurements were carried out by the reverse phase method, in which a C18 column was used as the stationary phase and a methanol:ethanol (70:30) mixture as the mobile phase. Each solution was injected into the HPLC instrument at a flow rate of 1 mL/min with the UV detector set at 212 nm. Then, the sample solution was injected into the instrument with the same parameters.

3. Results and Discussion

3.1 Synthesis and characterization of CIT-BCD

The CIT-BCD complex was synthesized through the esterification reaction between BCD and CIT. To prevent water particles from evaporating, the reaction was conducted in a closed vessel and placed in an oil bath whose temperature was kept at around 80–90 °C. The CIT-BCD compound was formed by reacting BCD with CIT without a catalyst, only by heating under fumigation conditions.

To confirm the formation of CIT-BCD, characterization using FTIR was carried out to verify the presence of functional groups formed during the reaction process. Figure 2 shows the IR spectra of BCD-CIT (purple line), CIT (green line), and BCD (blue line). The spectrum of CIT-BCD shows that there a shift in the C=O vibration absorption peak in CIT from the wave number of 1740 cm^{-1} to 1703 cm^{-1}, indicating the formation of an ester group from the carboxylate group and at the same time confirming the formation of the CIT-BCD conjugate via ester bonding.[22] The presence of the C=O vibration absorption peak at a wavelength of 1717 cm^{-1} was also

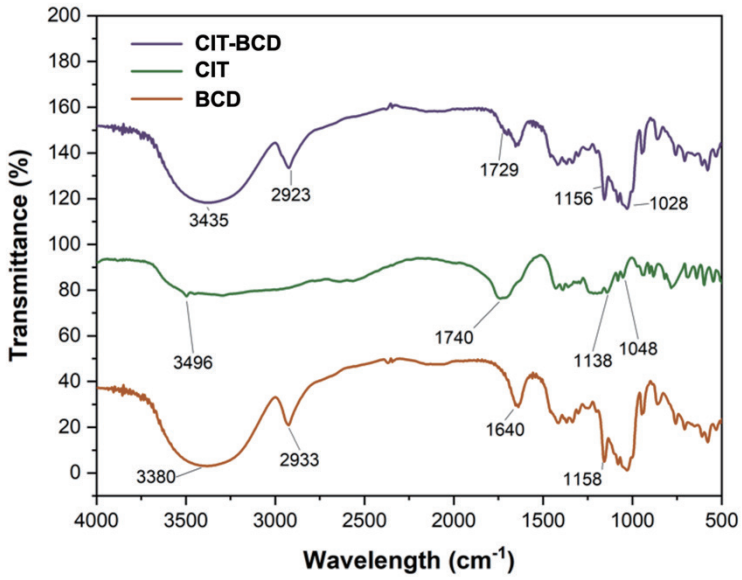

Fig. 2. (Color online) FTIR spectra of BCD, CIT, and CIT-BCD.

observed, suggesting the presence of carboxylate groups in CIT-BCD, where the -COOH groups attached to the C2 atom in the citrate groups. These results are in line with those of a previous study,[20] confirming the successful synthesis of the CIT-BCD conjugated compound.

3.2 Characterization of CIT-BCD@Fe_3O_4 nanocomposite

The CIT-BCD@Fe_3O_4 nanoparticles were prepared by coprecipitation. In principle, the Fe_3O_4 nanoparticles are formed by depositing ferric ions (Fe^{3+}) with ferrous ions (Fe^{2+}) at a molar ratio of 2:1 in alkaline solutions.[29,30] Fe_3O_4 was synthesized in vacuum to avoid contact with oxygen and prevent the formed Fe_3O_4 to be further oxidized to γ-Fe_2O_3.[19] The CIT-BCD@Fe_3O_4 nanocomposite was synthesized by mixing CIT-BCD and Fe_3O_4 nanoparticles in hot distilled water for 4 h. Excess CIT-BCD and impurities were then removed from the formed nanocomposites by collecting the latter with an external magnet. The CIT-BCD@Fe_3O_4 nanocomposite had a more brownish color than the Fe_3O_4 nanoparticles, revealing that CIT-BCD has been impregnated into the Fe_3O_4 nanoparticles.

To confirm the formation of Fe_3O_4 nanoparticles and CIT-BCD@Fe_3O_4 nanocomposites as well as to determine the crystallinity and theoretical average particle size, XRD analysis was performed. As shown in Fig. 3, the diffractogram of Fe_3O_4 nanoparticles shows typical peaks at 2θ (°) = 30.09 (220), 35.48 (311), 53.53 (422), 57.29 (511), and 62.71 (440), whereas the diffractogram of the CIT-BCD@Fe_3O_4 nanocomposite shows typical peaks at 2θ (°) = 30.24 (220), 35.64 (311), 53.66 (422), 57.16 (511), and 62.77 (440). The XRD results correspond to the typical peaks for each Miller index referred to the diffraction spectra of the spinel structure

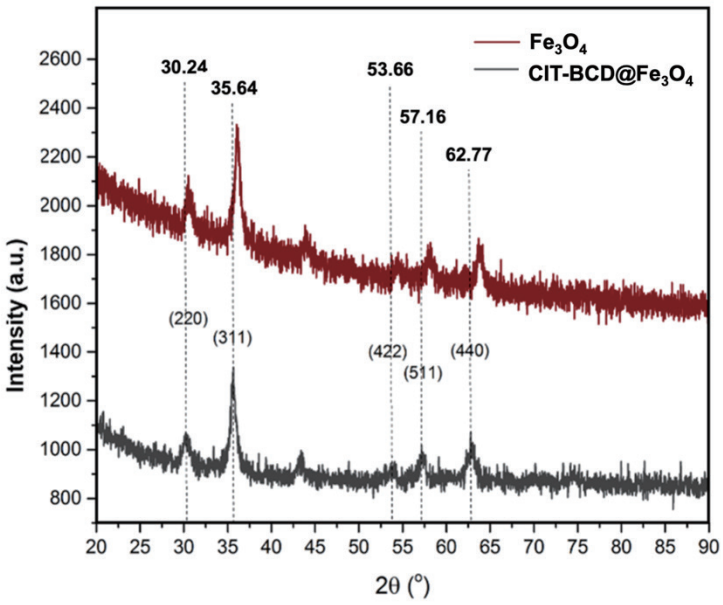

Fig. 3. (Color online) X-ray diffractograms of the synthesized Fe_3O_4 nanoparticles and CIT-BCD@Fe_3O_4 nanocomposite.

Fe_3O_4 on the JCPDS: 19-0629, which respectively have typical peaks at 2θ (°) = 30.10 (220), 35.42 (311), 53.39 (422), 56.94 (511), and 62.52 (440). The XRD results also confirm that the modification of Fe_3O_4 to form the CIT-BCD@Fe_3O_4 nanocomposite did not change the structure of Fe_3O_4. Furthermore, the average particle diameter was calculated from the observed peak of refraction from the Miller index (311) using the Scherrer equation.[31] From the results of this calculation, the particle sizes of the Fe_3O_4 nanoparticles and the CIT-BCD@Fe_3O_4 nanocomposite were determined to be 11.43 and 13.22 nm, respectively, which are consistent with the average particle size of Fe_3O_4 that is commonly formed by coprecipitation.

SEM characterization was also carried out to determine the morphology of both types of Fe_3O_4 nanoparticles and the CIT-BCD@Fe_3O_4 nanocomposite. Figure 4 shows the SEM images revealing that both types of Fe_3O_4 nanoparticles are spherical and agglomerate with each other. Furthermore, EDX analysis was carried out to determine the composition of the formed nanoparticles and nanocomposite as summarized in Table 1. Throughout the analysis, the synthesized Fe_3O_4 nanoparticles were validated to contain only two elements, Fe and O, confirming the purity of the formed nanoparticles. That is, there were no impurities such as N or

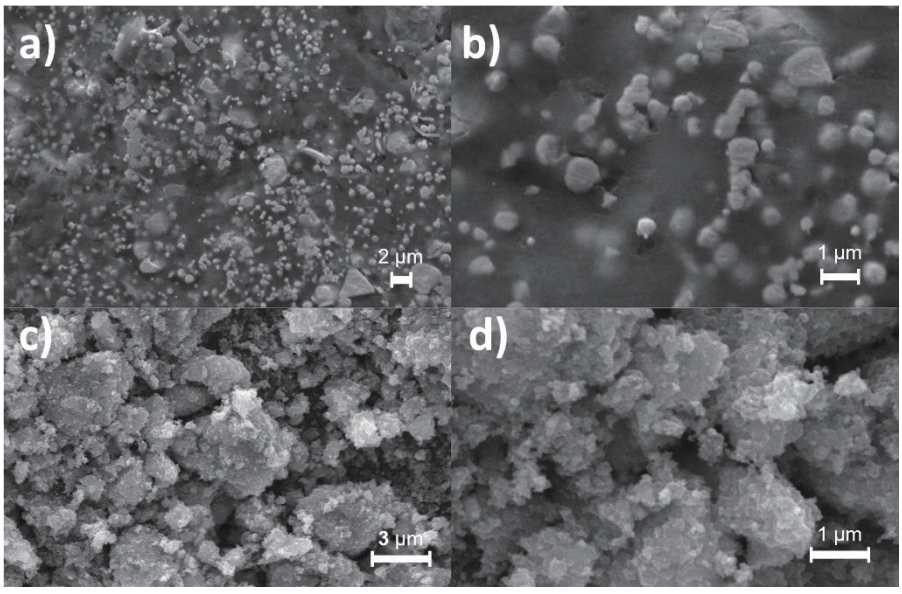

Fig. 4. (Color online) SEM images of the synthesized Fe_3O_4 nanoparticles with magnifications of (a) 2500× and (b) 10000× as well as the synthesized CIT-BCD@Fe_3O_4 nanocomposites with magnifications of (c) 5000× and (d) 15000×.

Table 1
Chemical compositions of Fe_3O_4 nanoparticles and CIT-BCD@Fe_3O_4 nanocomposite.

	Composition (%wt)		
	Fe	O	C
Fe_3O_4	64.8	35.2	—
CIT-BCD@Fe_3O_4	41.1	35.7	23.2

Cl, which may be present during the Fe_3O_4 formation. The carbon fraction was observed in CIT-BCD@Fe_2O_3. Furthermore, the EDX characterization confirmed the increase in C atomic composition in the sample, indicating the presence of CIT-BCD. The C atomic composition was observed to be 23.2%, whereas the Fe and O atomic compositions were 41.1 and 35.7%, respectively. Therefore, it can be affirmed from the results of SEM-EDX analysis that both Fe_3O_4 nanoparticles and the CIT-BCD@Fe_3O_4 nanocomposite have been successfully formed.

3.3 Molecular docking analysis

The docking simulation was carried out twice using the flexible docking method. In contrast to the rigid docking method, where ligands are assumed to be flexible and receptors are assumed to be rigid, following the principles of the lock-and-key theory, the flexible docking method refers to the approach that both ligands and receptors can move flexibly, in accordance with the induced-fit theory. However, to streamline the computational power required in the docking process, only atoms on the binding site of the receptor can move freely, whereas atoms far from the binding site of the receptor are still assumed to be rigid.[32–34] The results of the molecular docking simulation between BCD and CIT-BCD compounds with cholesterol and MB are shown in Table 2. From these results, cholesterol compounds are known to have $\Delta G_{binding}$ values of −5.70 and −6.40 kcal/mol against BCD and CIT-BCD receptors, with pK_d values of 4.20 and 4.71, respectively. The $\Delta G_{binding}$ and pK_d values were lower and higher for MB, with $\Delta G_{binding}$ and pK_d values of −4.90 kcal/mol and 3.61 (for BCD) and −5.30 kcal/mol and 3.90 (for CIT-BCD), respectively. These docking results confirmed that the presence of cholesterol will eventually substitute MB in the hydrophobic cavity of BCD. The cholesterol-BCD inclusion complex with a higher binding affinity and a more complex stability than the MB-BCD inclusion complex was formed. The release of the MB compound from the BCD complex will increase the MB concentration in the solution, which is assumed to be proportional to the added cholesterol concentration. The formation of MB oxidation and reduction current peaks through the CV technique will then be observed and analyzed to determine the cholesterol level in the solution, which can later be used to create a calibration curve to determine the regression equation for the oxidation and reduction peaks of MB as a basis for determining cholesterol levels in the test sample using the electrochemical method with the CV technique.

The analysis of the interaction between cholesterol and MB with BCD and CIT-BCD receptors is necessary to assess whether the molecular interactions that occurred as a result of docking simulation are in accordance with the hypothesis. Figures 5(a) and 5(b) show that the conformation of the cholesterol compound resembles the molecular conformation of the

Table 2
Docking simulation results of BCD and CIT-BCD with cholesterol and MB using flexible docking method.

Ligand	BCD		CIT-BCD	
	$\Delta G_{binding}$ (kcal/mol)	pK_d	$\Delta G_{binding}$ (kcal/mol)	pK_d
Cholesterol	−5.70	4.20	−6.40	4.71
Methylene blue	−4.90	3.61	−5.30	3.90

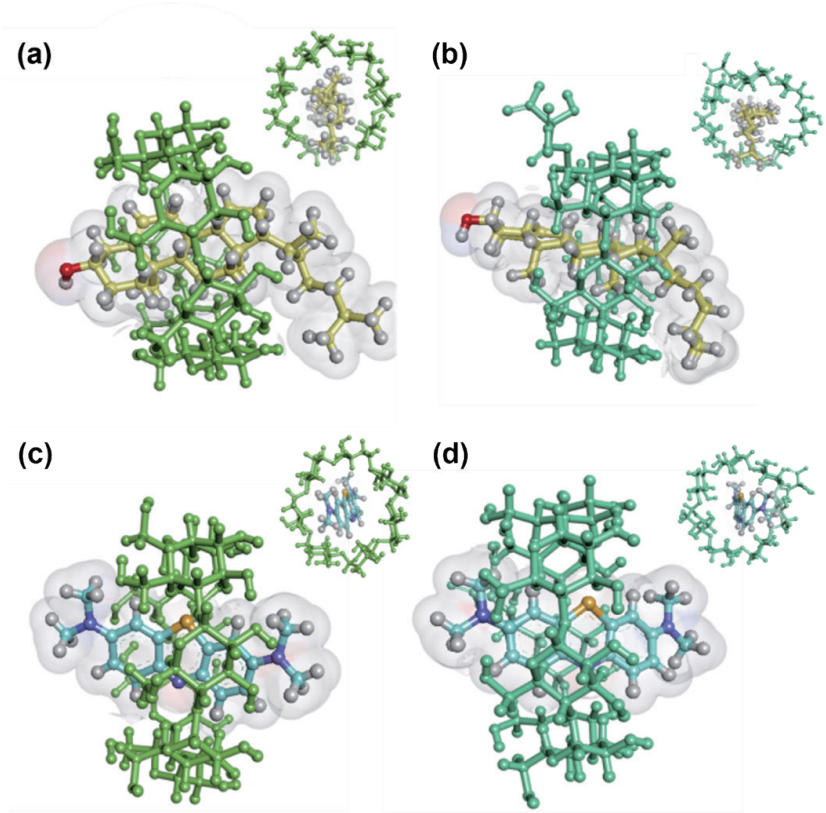

Fig. 5. (Color online) 3D visualization of the complex inclusion of cholesterol with (a) BCD, (b) CIT-BCD, (c) MB-BCD, and (d) MB-CIT-BCD.

cholesterol-BCD inclusion complex previously studied,[35] where the –OH group and hydrophilic tail on cholesterol enter the hydrophilic and hydrophobic cavities of BCD, respectively. Further analysis also revealed that the molecular interactions that occurred in the cholesterol-BCD complex inclusion were entirely van der Waals interactions between the hydrophobic sites of the sterol ring on cholesterol and the BCD hydrophobic pocket. Interestingly, from the visualization of cholesterol and the CIT-BCD complex, the sterol ring of cholesterol appeared to completely enter the hydrophobic cavity of CIT-BCD. This is probably because of two factors: (i) the hydrophobic and hydrophilic cavities of CIT-BCD being larger than those of BCD, such that the cholesterol molecules can enter into the deeper parts of the BCD hydrophobic cavity, and (ii) the effect of the modified citrate group from CIT-BCD, which allows the effect of van der Waals interactions on cholesterol molecules. These factors are considered to have a major effect on the increased binding affinity of cholesterol when interacting with CIT-BCD with BCD.

The docking simulations of MB against the BCD and CIT-BCD receptors, as shown in Figs. 5(c) and 5(d), respectively, revealed that there was no significant change between the interactions of MB with BCD both before and after citrate modification. As with cholesterol, the interaction of MB-BCD and MB/CIT-BCD complexes was also markedly dominated by van der Waals and hydrophobic interactions. However, in the MB-BCD complex, there was a π-cationic interaction

between the aromatic ring of MB and the polar hydrogen atom on the C6 carbon atom in one of the glucose rings. This is possible because the aromatic ring is an electron-rich species owing to the effect of resonance, whereas the hydrogen atom on the C6 carbon atom tends to be electropositive owing to the effect of the –OH functional group around the carbon atom. Furthermore, the docking results of the CIT-BCD inclusion complex with MB also showed that there was a π-cationic interaction between the MB aromatic ring and the hydrogen atom in the –OH group in one of the CIT-BCD glucose chains. Because the polar hydrogen atom in –OH is more electropositive than the hydrogen atom covalently bonded to the carbon atom, the π-cationic interaction between MB and CIT-BCD was stronger than that of MB and BCD. This also increases the overall binding affinity that occurs between MB and CIT-BCD complexes compared with MB and BCD complexes. Moreover, the increase in the affinity of MB at the CIT-BCD receptor compared with BCD is possible owing to the effect of the citrate group, which makes the CIT-BCD more stable and has an additional effect on the occurrence of van der Waals and hydrophobic interactions with MB.

3.4 Electrochemical measurement results

Basically, the electrochemical measurements in this work are performed to detect the release of MB from the system after contacting MB/CIT-BCD@Fe_3O_4 with cholesterol. Typically, a couple of oxidation-reduction peaks of MB at potentials of around +0.47 and −0.43 V are observed.[28] Figure 6(a) shows cyclic voltammograms of the release of MB in 50 mM PBS (pH 7.4) in the absence (dashed line) and presence (solid line) of 100 μM cholesterol after contacting the MB-modified@Fe_3O_4 particles, without BCD or citrate. The presence of cholesterol in the solution employing the unmodified Fe_3O_4 systems did not significantly change the release of MB as indicated by the similar current responses in voltammograms. On the contrary, the modification of the Fe_3O_4 particles with citrate, BCD, and MB increased the current response of MB in solution [Fig. 6(b)]. This result indicates the increase in the release of MB from BCD due to the higher affinity of cholesterol than of MB to BCD.

Furthermore, the concentration of CIT-BCD in Fe_3O_4 was optimized by measuring the MB current response by cyclic voltammetry in the presence of cholesterol. The presence of cholesterol in the electrochemical measurement increased the current response with the increase in CIT-BCD concentrations from 1 to 3%. The highest current response in signal-to-background ratio (ΔI) was achieved in 3% (w/w) CIT-BCD with 10 times higher cathodic response (ΔI) at the potential of −0.43 V than that in the unmodified Fe_3O_4 [Fig. 6(b)]. The probable reason is the increase in the number of electroactive sites with better interaction in CIT-BCD with cholesterol, resulting in the increase in the release of MB. These results are in line with the molecular docking data, where the presence of CIT-BCD molecules increases the binding strength between the aromatic ring from cholesterol and –OH at the glucose chain. Additionally, the cathodic current response provides a better signal-to-background ratio (ΔI) than the anodic current response, which is clearly observed in Fig 6, suggesting a higher detection sensitivity caused by using the cathodic current.

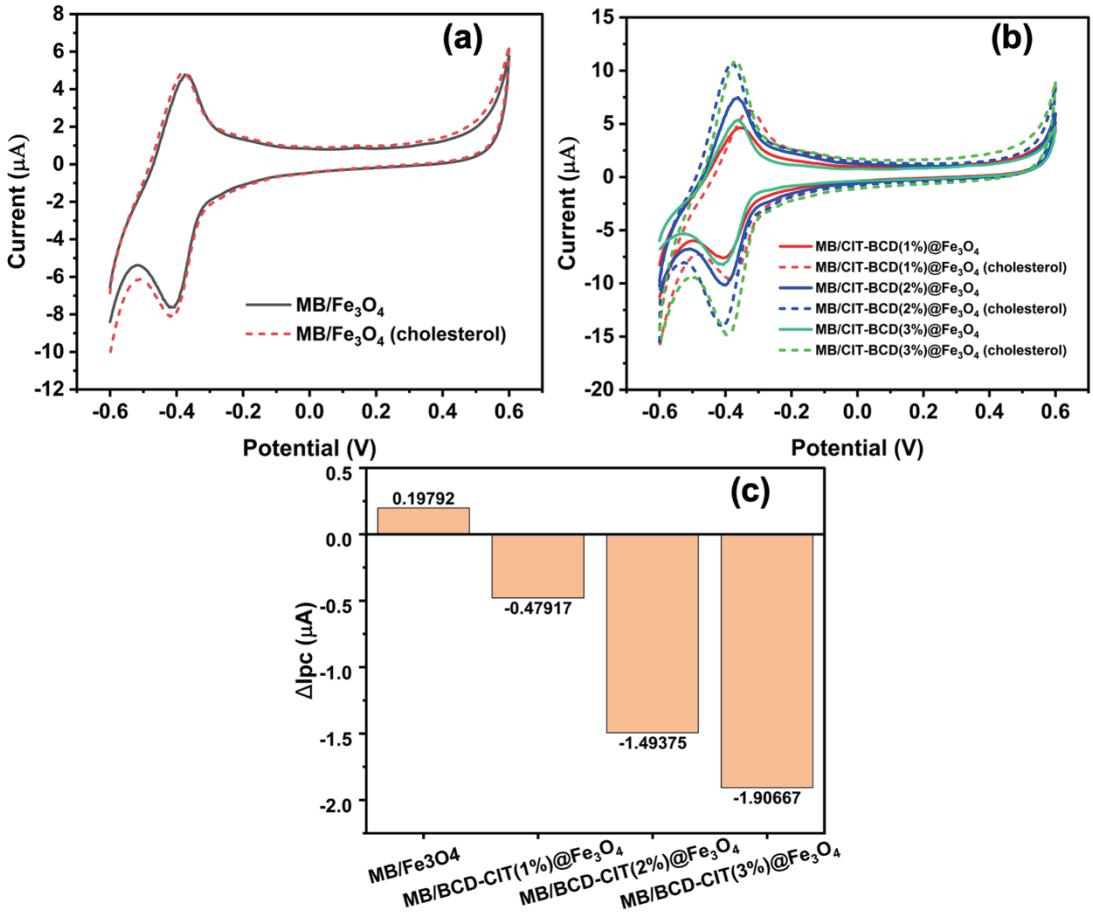

Fig. 6. (Color online) Voltammograms of the release of MB in 50 mM PBS in the absence (dashed line) and presence (solid line) of 100 μM cholesterol after 10 min contact with the MB-modified Fe_3O_4 systems without BCD or citrate (a) and with the various amounts of MB/CIT-BCD@Fe_3O_4 (b) together with the curve of signal-to-background ratio (ΔI) extracted from (a) and (b). The scan rate of the voltammograms was fixed at 40 mV·s^{-1}.

The optimum potential was studied by observing the slope of the transfer function equation to determine the sensitivity of the amperometry method (Fig. S1) to various predetermined potential variations shown in Fig. 7(a). The transfer function is described as[36]

$$S = A + Bx, \tag{1}$$

where S = electrical signal generated by the sensor = current response (μA), A = sensor offset (μA), B = slope sensor (μA/μM), and x = units calculated = concentration of analyte (μM).

By comparing the linear equations at different potentials in Table 3, we found that the potential of −0.43 V produced the highest slope at −0.02 μA/μM with a relative high offset at 0.35 A. The offset is the current generated by the sensor when no analyte is added to the system.[36] There is a tendency that the offset of the amperometry sensor increases as the potential used decreases.

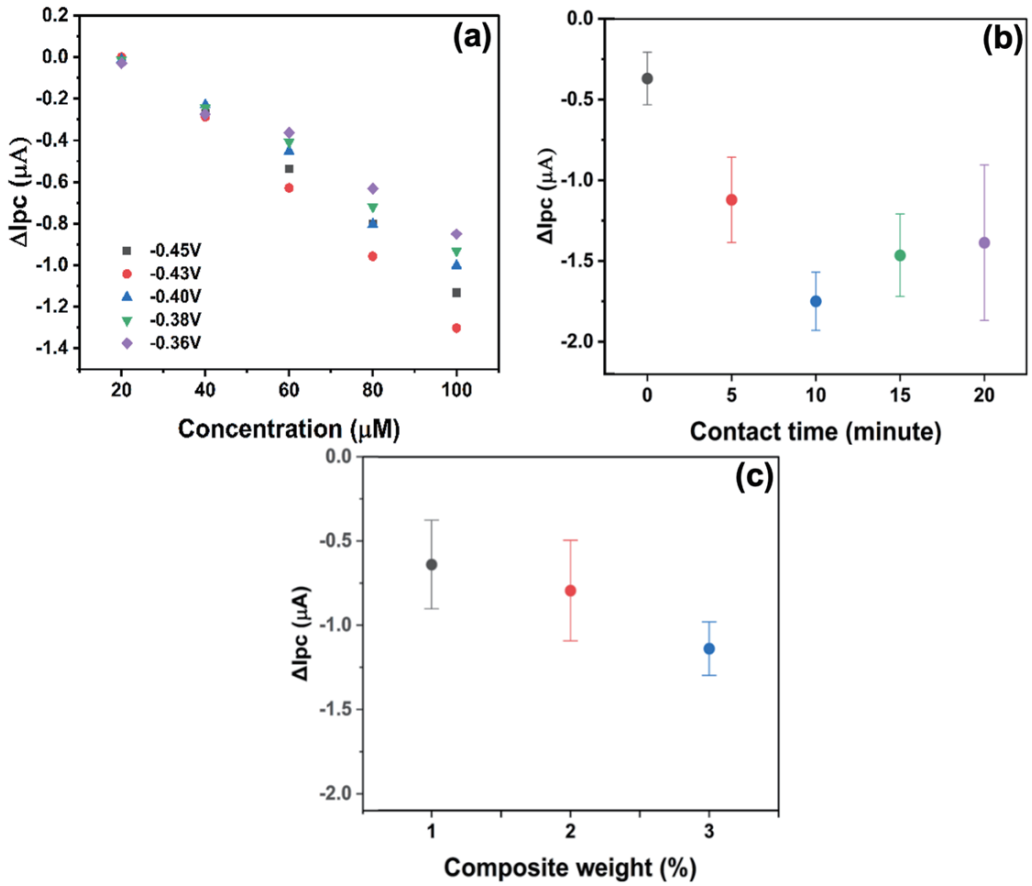

Fig. 7. (Color online) Current dependence of 100 μM standard cholesterol solution after contact with the MB/CIT-BCD@Fe_3O_4 composite at (a) various applied potentials, (b) contact times, and (c) composite weights.

Table 3
Comparison of linear equations of the current response of nanocomposite-based cholesterol sensor at various potentials determined by the amperometry method.

Applied potential (V)	Current response	
	Linear equation	R^2
−0.45	$y = -0.01x + 0.28$	0.99
−0.43	$y = -0.02x + 0.35$	0.99
−0.40	$y = -0.01x + 0.01$	0.99
−0.38	$y = -0.01x + 0.08$	0.99
−0.36	$y = -0.01x + 0.17$	0.98

The contact time between the cholesterol solution and the MB/CIT-BCD@Fe_3O_4 composite is also one of the main factors that must be optimized to achieve good performance in the cholesterol detection as it affects the interaction between cholesterol and BCD and also the release of MB from its interaction with BCD. The dissociation reaction and the interference of other molecules can decrease the sensor performance, so this issue must be resolved by controlling the reaction time to produce good sensor measurement. Figure 7(b) shows that the

optimum contact time was 10 min after contact between MB/CIT-BCD@Fe_3O_4 and the cholesterol solution. This finding indicates that an increase in contact time by more than 10 min gives a lower current response as the deformation system, which is formed by the strong interaction between cholesterol and the CIT-BCD species composite structure, induces the release of MB to the electrolyte system. Additionally, the increase in composite weight also affected the measurement sensitivity of the sensor. Figure 7(c) shows that the highest current response was achieved at the composite weight of 3%, which might be due to the fact that the loading of a higher composite mass increased the capability of the sensor to interact with total cholesterol in the solution.

Figure 8(a) shows the amperometric measurements of the standard cholesterol solutions in the concentration range from 0 to 100 μM. The measurements were performed at a potential of −0.43 V for 90 s with data collection intervals of 0.5 s. The calibration curve in Fig. 8(b) shows that a linear increase in current response to the cholesterol concentration can be achieved with good linearity ($R^2 > 0.99$) and a regression equation of I (μA) = −0.02 [cholesterol] (μM) − 0.20. From the calculation results, the limit of detection (LOD) and the limit of quantification (LOQ) are determined to be 3.93 and 13.10 μM, respectively. Good measurement repeatability was also observed in seven replications with a relative standard deviation of 5.98% as shown in Fig. 8(b), indicating that the developed sensor is promising for the actual detection of cholesterol

3.5 Corned beef sample measurement

Prior to the electrochemical measurements of cholesterol in the corned beef sample, an interference study was conducted for the compounds possibly contained in the corned beef sample, such as ascorbic acid, palmitic acid, arginine, isoleucine, tyrosine, and threonine, which

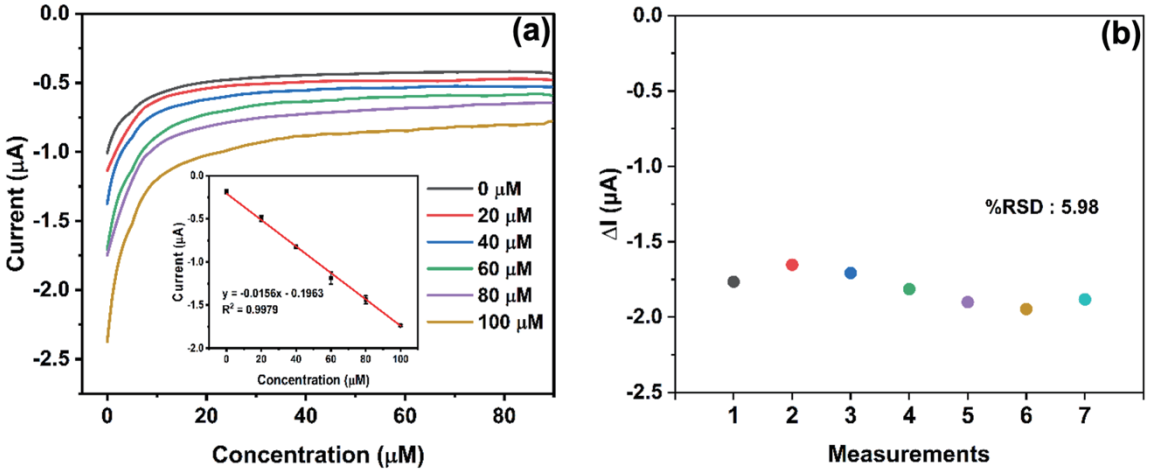

Fig. 8. (Color online) (a) Amperometric voltammograms of the standard cholesterol solutions of various concentrations in the range between 0 and 100 μM employing MB/CIT-BCD(3%)@Fe_3O_4 at an applied potential of −0.43 V and (b) the repeatability performance of sensor in seven replications. The inset shows the calibration curve extracted from (a).

might interfere with the sensor performance. As seen in the graph in Fig. 9, the addition of arginine to the solution increases the current response by 275.25–283.34% for the CIT-BCD@Fe_3O_4 nanocomposite and 60.18–161.67% for the BCD@Fe_3O_4 nanocomposite. The probable reason is the presence of arginine with a positively charged amino acid that is also electroactive. In addition, arginine was reported to strongly interact with the CIT-BCD cavity to form inclusion complexes through the primary –OH interaction.[37] Hence, arginine significantly interferes with the measurements.

Isoleucine has the highest current response after arginine with current responses of 3.03–14.00% for the CIT-BCD@Fe_3O_4 nanocomposite and 45.56–50.73% for the BCD@Fe_3O_4 nanocomposite. This high current response is due to the classification of isoleucine as a polar amino acid. In the case of threonine, current responses of −8.42 to −4.00% for the CIT-BCD@Fe_3O_4 nanocomposite and −8.15 to −5.06% for the BCD/Fe_3O_4 nanocomposite were observed because of its characteristic properties as an aliphatic nonpolar amino acid. Moreover, tyrosine had current responses of −14.95 to −5.67% for the CIT-BCD@Fe_3O_4 nanocomposite and −15.96 to −13.62% for the BCD@Fe_3O_4 nanocomposite. As tyrosine is an aromatic nonpolar amino acid, it is difficult to be ionized. The presence of CIT-BCD on the prepared sensor revealed a good effect on the selectivity of detection. This phenomenon was induced by synergistic interaction between the citric functional group and BCD, which made the binding between BCD and cholesterol stronger than that between BCD and MB. This mechanism generated the signal response in the cholesterol detection. Moreover, the presence of CIT-BCD@Fe_3O_4 [Fig. 9(b)] enhances the selectivity performance of the sensor in the presence of excess arginine molecules during the measurement compared with that observed in the absence of both molecules [Fig. 9(a)].

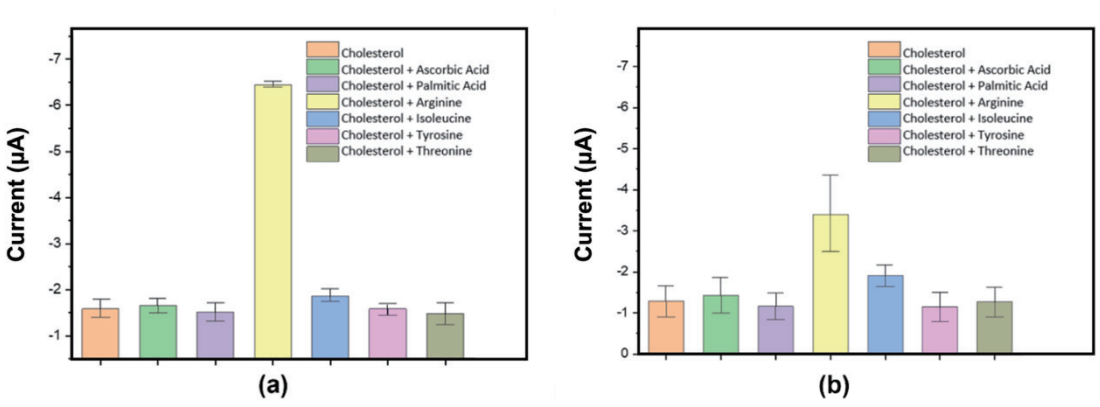

Fig. 9. (Color online) Diagram of current responses extracted from the measurements of 100 μM standard cholesterol solutions in the absence and presence of 100 μM interfering compounds using amperometry technique after contact with (a) BCD-CIT(3%)@Fe_3O_4 and (b) BCD@Fe_3O_4 nanocomposites. The measurements were conducted using one single electrode under the same conditions as in Fig. 8.

To determine the cholesterol level in the commercial corned beef sample, analysis was carried out using an HPLC instrument. Initially, a calibration curve was created in the concentration range from 0 to 100 μM. The cholesterol peak on the HPLC chromatogram was found at t_r = 11.45 min, indicated by the increase in peak with the addition of the standard cholesterol concentrations. From the measurements, the calibration curve was used to obtain the following equation: Peak area (mAu min) = 1330 [cholesterol] (μM) – 1587 with a good linear regression value of R^2 = 0.99. HPLC measurements performed on samples produced a complex chromatogram showing various peaks, indicating the presence of other nonpolar compounds, such as fatty acids. These peaks were found at retention times of 0.92, 2.38, 2.60, 5.13, 5.40, 10.68, and 11.38 min. The peak corresponding to cholesterol was found at a retention time of 11.38 min with a peak area of 65368 mAu min. From the HPLC results, the cholesterol level obtained in the sample with 2× dilution was 50.40 μM.

The cholesterol level in the commercial corned beef sample was also examined by using the developed sensors. From the amperometric measurements, the average current difference was determined to be 0.071 μA. The calculation using the standard calibration curve showed that the cholesterol level in the sample diluted twice was 50.60 μM (Fig. 10). The difference at around 1.50% from the conventional detection indicates that both results are comparable. Furthermore, from measurements using spike cholesterol with a concentration of 40 μM, the average current of 1.079 was observed, suggesting the cholesterol content of 88.46 μM (Fig. 10). The recovery obtained was at 98.24%. The results indicate that the sensor can be used for actual applications in the detection of cholesterol in food samples. The summary of the cholesterol measurements is presented in Table 4.

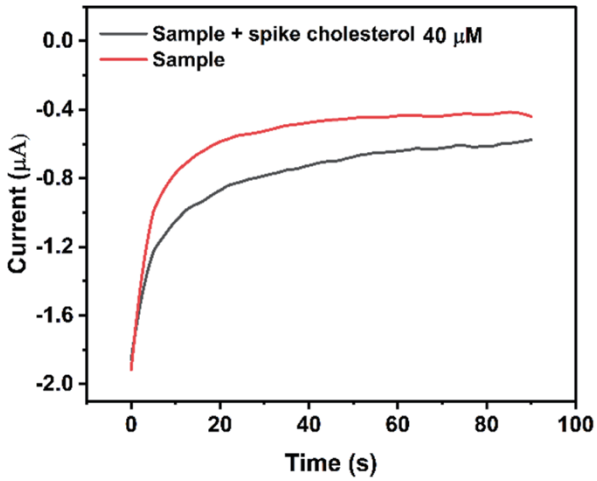

Fig. 10. (Color online) Amperometric voltammograms of cholesterol detection in the cornet beef sample with and without the addition of 40 uM standard cholesterol.

The method of detecting cholesterol species using an advance electrocatalyst material was well developed by many researchers using enzymatic and non-enzymatic sensor pathways. In this research, the prepared MB-CIT-BCD@Fe_3O_4 composite as a non-enzymatic cholesterol sensor exhibited good performance in terms of selectivity and LOD, and the result was consistent with the data of the computation previously performed. Furthermore, the performance of the developed sensor was excellent compared with that of the other reported sensors developed by methods using enzymatic pathways,[38,40,42] which is a favorable result compared with that of the other developed sensor using β-cyclodextrins in their measurement.[28,39] Additionally, the differences in synthesis pathway and electrochemical measurement are the probable reasons that make the sensitivity of MB/CIT-BCD@Fe_3O_4 become three times higher than that of MB/BCD-CIT@Fe_3O_4 even though at the same material composition. This result is attributed to the different electrochemical procedure used (CV or amperometry). In CV, the current response was produced by potential scanning in the determined potential range; this mechanism makes the reaction with other species interfere with the measurement. In contrast, in amperometry, the current response was only generated by the specific potential applied to control a specific reaction during sensor measurement.[43,44] The comparison in Table 5 suggests that our developed sensor provides comparable performance to the other previously reported sensors. However, this proposed MB/CIT-BCD@Fe_3O_4 sensor has more potential advantages as a non-enzymatic sensor, which can be produced commercially at a lower cost than an enzymatic sensor.

Table 4
Cholesterol contents in corned beef samples measured by various methods.

Methods	Spike (μM)	Linear equation	Detected [cholesterol] (μM)	Recovery (%)
HPLC	0	$y = 1330x - 1587$	50.04	—
Amperometry	0	$y = -0.02x - 0.20$	50.06	—
	40		88.46	98.24

Table 5
Comparison of some reported sensor developments in cholesterol detection.

Sensor	Methods	Linearity range (μM)	LOD (μM)	Sensitivity
ChOx/CHER/AuNPs/SPCE[38]	LSV	12886–12886000	7731	0.0610 μA/μg mL^{-1}
N-QDG/benzoquinon/β-cyclodextrins[39]	DPV	0–85	2.10	0.0201 μA/μM
	Fluorescence	0–85	2.90	74.7204 a.u/μM
TiO_2 nanotube/graphite pencil[40]	Amperometry	3000–10000	4480	NA
MB/BCD-CIT/Fe_3O_4[28]	CV	0–150	2.88	0.0043 μA/μM
Chox-nanoporous gold/SPCE[41]	CV	50–6000	8.36	32.68 μA mM^{-1} cm^{-2}
ChOx-ChE/Fe_3O_4[42]	CV	644.33–12886.60	500	0.0039 μA/mg dL^{-1}
MB/CIT-BCD@Fe_3O_4/SPCE (This work)	Amperometry	0–100	3.93	0.02 μA/μM

LSV: linear sweep voltammetry, DPV: difference pulse voltammetry, and CV: cyclic voltammetry.

4. Conclusions

The composite of citrate-β-cyclodextrin-Fe_3O_4 (CIT-BCD@Fe_3O_4) was successfully synthesized by coprecipitation. The spinel structure with an average particle diameter of around 13.22 nm was confirmed by XRD and TEM characterization. The optimum conditions for cholesterol measurements obtained on the basis of the inclusion complex formation of MB and cholesterol with CIT-BCD@Fe_3O_4 suggested the utilization of the 3% (w/w) CIT-BCD(3%)@Fe_3O_4 nanocomposite in the detection system with a contact time of 10 min. The amperometric measurements using an SPCE electrode showed good linearity ($R^2 > 0.99$) in the concentration range of 0–100 μM with the linear equation of I (μA) = –0.02[cholesterol] (μM) – 0.20. An LOD of 3.93 μM, an LOQ of 13.05 μM, and a sensitivity of 0.02 or 0.12 μA/μM cm^2 could be achieved. Computational studies with docking simulation indicate that citrate-β-cyclodextrin has better molecular interactions as well as higher binding affinities toward cholesterol and MB than the unmodified β-cyclodextrin. Furthermore, the developed sensors have good selectivity for ascorbic acid, palmitic acid, tyrosine, and threonine, whereas it was interfered by arginine. The developed sensor was also successfully demonstrated for the measurement of the cholesterol level in commercial corned beef samples, showing results comparable to HPLC measurements. The results indicate that the developed sensors can be used for cholesterol detection in food samples.

Acknowledgments

This research was funded by the Ministry of Research and Technology/National Research and Innovation Agency, Republic of Indonesia, through Hibah Penelitian Dasar Unggulan Perguruan Tinggi 2021 with grant no. NKB-173/UN2.RST/HKP.05.00/2021.

Author Contributions

Conceptualization: Mochammad Arfin Fardiansyah Nasution, Tribidasari Anggraningrum Ivandini; Methodology: Mochammad Arfin Fardiansyah Nasution, Tribidasari Anggraningrum Ivandini; Formal analysis and investigation: Mochammad Arfin Fardiansyah Nasution, Metya Indah Firmanti, Hanzhola Gusman Riyanto, Afiten Rahmin Sanjaya; Validation: Tribidasari Anggraningrum Ivandini; Writing - original draft preparation: Mochammad Arfin Fardiansyah Nasution, Metya Indah Firmanti, Hanzhola Gusman Riyanto, Afiten Rahmin Sanjaya; Writing - review and editing: Endang Saepudin, Tribidasari Anggraningrum Ivandini; Funding acquisition and resources: Tribidasari Anggraningrum Ivandini; Supervision: Endang Saepudin, Tribidasari Anggraningrum Ivandini.

Competing Interests

The authors also have no conflicts of interest to disclose regarding the publication of this research article.

References

1 WHO: Cardiovascular Diseases https://www.who.int/health-topics/cardiovascular-diseases/#tab=tab_1 (accessed: Nov. 16, 2023).
2 N. Mboi, I. M. Surbakti, I. Trihandini, I. Elyazar, K. H. Smith, P. B. Ali, S. Kosen, K. Flemons, S. E. Ray, J. Cao, S. D. Glenn, M. K. M. Petrie, M. D. Mooney, J. L. Ried, D. N. A. Ningrum, F. Idris, K. N. Siregar, P. Harimurti, R. S. Bernstein, T. Pangestu, Y. Sidharta, M. Naghavi, C. J. L. Murray, and S. I. Hay: Lancet **392** (2018) 581. https://doi.org/10.1016/S0140-6736(18)30595-6
3 G. Jagadeesh, P. Balakumar, and K. Maung-U: Pathophysiology and Pharmacotherapy of Cardiovascular Disease (Springer International Publishing, 2015). https://doi.org/10.1007/978-3-319-15961-4
4 S. I. Sulimovici and G. S. Boyd: Vitamins & Hormones **27** (1970) 199. https://doi.org/10.1016/S0083-6729(08)61127-9
5 P. C. Deedwania, E. V. Carbajal, and V. R. Bobba: Clin. Cardiol. **30** (2007) I16. https://doi.org/10.1002/clc.20049
6 T. T. N. Dinh, L. D. Thompson, M. L. Galyean, J. C. Brooks, K. Y. Patterson, and L. M. Boylan: Compr. Rev. Food Sci. Food Saf. **10** (2011) 269. https://doi.org/10.1111/j.1541-4337.2011.00158.x
7 N. R. Nirala, S. Abraham, V. Kumar, A. Bansal, A. Srivastava, and P. S. Saxena: Sens. Actuators, B **218** (2015 42. https://doi.org/10.1016/j.snb.2015.04.091
8 H. M. Lotfy and M. A. M. Hegazy: Spectrochim Acta A Mol. Biomol. Spectrosc. **113** (2013) 107. https://doi.org/10.1016/j.saa.2013.04.064
9 V. Narwal, R. Deswal, B. Batra, V. Kalra, R. Hooda, M. Sharma, and J. S. Rana: Steroids **143** (2019) 6. https://doi.org/10.1016/j.steroids.2018.12.003
10 U. Saxena and A. B. Das: Biosens. Bioelectron. **75** (2016) 196. https://doi.org/10.1016/j.bios.2015.08.042
11 S. S. Jambhekar and P. Breen: Drug Discov. Today **21** (2016) 356. https://doi.org/10.1016/j.drudis.2015.11.017
12 T. Ogoshi and A. Harada: Sensors **8** (2008) 4961. https://doi.org/10.3390/s8084961
13 Y. Zhou, C. Wang, F. Wang, C. Li, C. Dong, and S. Shuang: Chin. J. Chem. **34** (2016) 599. https://doi.org/10.1002/cjoc.201500756
14 S. Soylemez, S. O. Hacioglu, M. Kesik, H. Unay, A. Cirpan, and L. Toppare: ACS Appl. Mater. Interfaces **6** (2014) 18290. https://doi.org/10.1021/am5054493
15 M. Arvand, Sh. Sohrabnezhad, M. F. Mousavi, M. Shamsipur, and M. A. Zanjanchi: Anal. Chim. Acta **491** (2003) 193. https://doi.org/10.1016/S0003-2670(03)00790-6
16 Y. Wu, F. Zuo, Z. Zheng, X. Ding, and Y. Peng: Nanoscale Res. Lett. **4** (2009) 738. https://doi.org/10.1007/s11671-009-9314-x
17 A. P. F. Monteiro, L. D. Caminhas, J. D. Ardisson, R. Paniago, M. E. Cortés, and R. D. Sinisterra: Carbohydr. Polym. **163** (2017) 1. https://doi.org/10.1016/j.carbpol.2016.11.091
18 V. S. Ghorpade, A. V. Yadav, and R. J. Dias: Int. J. Biol. Macromol. **93** (201) 75. https://doi.org/10.1016/j.ijbiomac.2016.08.072
19 H. Wang, Y. Zhou, Y. Guo, W. Liu, C. Dong, Y. Wu, S. Li, and S. Shuang: Sens. Actuators, B **163** (2012). https://doi.org/10.1016/j.snb.2012.01.031
20 K. N. Jayaprabha and P. A. Joy: RSC Adv. **5** (2015) 22117. https://doi.org/10.1039/C4RA16044D
21 M. A. F. Nasution, H. G. Riyanto, E. Saepudin, and T. A. Ivandini: IOP Conf. Ser. Mater. Sci. Eng. **902** (2020) 012017. https://doi.org/10.1088/1757-899X/902/1/012017
22 K. Eltahlawy, M. Gaffar, and S. Elrafie: Carbohydr. Polym. **63** (2006) 385. https://doi.org/10.1016/j.carbpol.2005.08.057
23 E. Saepudin, S. J. Willyam, Irkham, and T. A. Ivandini: IOP Conf. Ser. Mater. Sci. Eng. **902** (2020) 012005. https://doi.org/10.1088/1757-899X/902/1/012005
24 S. Kim, P. A. Thiessen, T. Cheng, B. Yu, B. A. Shoemaker, J. Wang, E. E. Bolton, Y. Wang, and S. H. Bryant: J. Cheminf. **8** (2016) 32. https://doi.org/10.1186/s13321-016-0142-6
25 N. M. Koropatkin, E. C. Martens, J. I. Gordon, and T. J. Smith: Structure **16** (2008) 1105. https://doi.org/10.1016/j.str.2008.03.017
26 S. Ejaz, H. Nadeem, R. Z. Paracha, S. Sarwar, and S. Ejaz: BMC Chem. **13** (2019) 115. https://doi.org/10.1186/s13065-019-0631-6
27 M. A. Isa, R. S. Majumdhar, and S. Haider: J. Mol. Model **24** (2018) 132. https://doi.org/10.1007/s00894-018-3637-4
28 S. J. Willyam, E. Saepudin, and T. A. Ivandini: Anal. Methods **12** (2020) 3454. https://doi.org/10.1039/D0AY00933D

29 N. Sinan and E. Unur: Mater. Chem. Phys. **183** (2016) 571. https://doi.org/10.1016/j.matchemphys.2016.09.016.
30 J. Safari, Z. Zarnegar, and H. Hekmatara: Synth. React. Inorg. Met.-Org. Nano-Metal Chem. **46** (2016) 1047. https://doi.org/10.1080/15533174.2013.776597
31 A. L. Patterson: Phys. Rev. **56** (1939) 978. https://doi.org/10.1103/PhysRev.56.978
32 N. M. F. S. A. Cerqueira, D. Gesto, E. F. Oliveira, D. S. Martins, N. F. Brás, S. F. Sousa, P. A. Fernandes, and M. J. Ramos: Arch. Biochem. Biophys. **582** (2015) 56. https://doi.org/10.1016/j.abb.2015.05.011.
33 P. Englebienne and N. Moitessier: J. Chem. Inf. Model **49** (2009) 2564. https://doi.org/10.1021/ci900251k
34 C. F. Wong: Expert Opin. Drug Discov. **10** (2015) 1189. https://doi.org/10.1517/17460441.2015.1078308
35 Y. Yu, C. Chipot, W. Cai, and X. Shao: J. Phys. Chem. B **110** (2006) 6372. https://doi.org/10.1021/jp056751a
36 M. J. McGrath and C. N. Scanaill: Sensor Technologies (Berkeley, CA, Apress, 2013) pp. 15–50. https://doi.org/10.1007/978-1-4302-6014-1_2
37 F. Zhang, S. Gu, Y. Ding, Z. Zhang, and L. Li: Anal. Chim. Acta **770** (2013) 53. https://doi.org/10.1016/j.aca.2013.01.052
38 Y. Huang, L. Cui, Y. Xue, S. Zhang, N. Zhu, J. Liang, and G. Li: Mater. Sci. Eng. C **77** (2017) 1. https://doi.org/10.1016/j.msec.2017.03.253
39 W. Aidli, V. Pifferi, A. Mars, D. Marinotto, M. Longhi, A. Manfredi, A. H. Hamzaoui, and L. Falciola: Electrochim. Acta **464** (2023) 142936. https://doi.org/10.1016/j.electacta.2023.142936
40 B. Batra, V. Narwal, Sumit, J. Ahlawat, and M. Sharma: Sens. Int. **2** (2021) 100111. https://doi.org/10.1016/j.sintl.2021.100111
41 S. Wang, S. Chen, K. Shang, X. Gao, and X. Wang: Int. J. Biol. Macromol. **189** (2021) 356. https://doi.org/10.1016/j.ijbiomac.2021.08.145
42 W.-C. Shih, M.-C. Yang, and M. S. Lin: Biosens. Bioelectron. **24** (2009) 1679. https://doi.org/10.1016/j.bios.2008.08.055
43 T. A. Ivandini, W. P. Wicaksono, E. Saepudin, B. Rismetov, and Y. Einaga: Talanta **134** (2015) 136. https://doi.org/10.1016/j.talanta.2014.11.010
44 A. Preechaworapun, T. A. Ivandini, A. Suzuki, A. Fujishima, O. Chailapakul, and Y. Einaga: Anal. Chem. **80** (2008) 2077. https://doi.org/10.1021/ac702146u